

Heterogeneous interfacial failure between two elastic blocks

G. George Batrouni

Institut Non-Linéaire de Nice, UMR CNRS 6618, Université de Nice-Sophia Antipolis, 1361 Route des Lucioles, F-06560 Valbonne, France

Alex Hansen*

NORDITA and Niels Bohr Institute, Blegdamsvej 17, DK-2100 Copenhagen Ø, Denmark

Jean Schmittbuhl

Département de Géologie, UMR CNRS 8538, Ecole Normale Supérieure, 24, rue Lhomond, F-75231 Paris Cédex 05, France

(Received 19 July 2001; published 27 February 2002)

We investigate numerically the failure process when two elastic media, one hard and one soft that have been glued together thus forming a common interface, are pulled apart. We present three main results: (1) The area distribution of simultaneously failing glue (bursts) follows a power law consistent with the theoretically expected exponent 2.5, (2) the maximum load and displacement before catastrophic failure scale as L^2 and L^0 , respectively, where L is the linear size of the system, and (3) the area distribution of failed glue regions (clusters) is a power law with exponent -1.6 when the system fails catastrophically.

DOI: 10.1103/PhysRevE.65.036126

PACS number(s): 81.40.Pq, 83.80.Ab, 62.20.Mk, 81.40.Np

I. INTRODUCTION

The failure of interfaces under stress is a problem that has obvious important technological relevance. In addition, from a more fundamental point of view, this problem exhibits very interesting features. It is the aim of this paper to bring out some of these features by means of a numerical model based on a discretization of the original problem.

For more than a decade, failure processes in different contexts have caught the attention of the physics community. For a considerably longer period, the mechanics community has been involved in the study of such phenomena. In order to place the present study in its proper context, we need to go back to 1926 with the study of Peirce on what today is known as the *equal load-sharing fiber bundle* [1]. This consists of N parallel fibers, each with its own breaking threshold and connected in such a way that when a fiber fails, the load it was carrying would be distributed equally among all the surviving fibers. In 1945, Daniels published a very thorough study of this model, which today forms the starting point of any excursion into this field [2], where among other results, he presented its average load-deformation characteristics. The model has since these early days been generalized in many directions, one of which consists in replacing the “democratic” load-sharing rule by different local ones. One much studied variant is the *local load-sharing model*, where the load on the failing fiber is distributed equally among the nearest surviving fibers [3–6]. Results on, e.g., the average load-deformation characteristics of the local load-sharing model may be found in Refs. [6–8]. There has also been several studies of time-dependent phenomena in connection with the two variants of the fiber bundle model, see Ref. [9]. (This paper in addition contains a very thorough review of

the literature in this field.) There are also a number of studies “on the market” that may be placed between the two extremes of equal and local load-sharing models. Among them, we find the early study by Newman and Gabrielov [10], who constructed a hierarchically connected fiber bundle. Other work on hierarchical fiber bundle models may be found in Refs. [11–13].

Much work by the physics community has gone into studying network models, of which the *fuse model* is the most well known [14,15]. This model consists of a network of electrical fuses where their burn-out thresholds have been drawn from some probability distribution. This model may be regarded as yet another generalization of the fiber bundle model, however, this time along the axis on which we find chains of fiber bundles [16]. Among the several interesting questions that have been studied in connection with the fuse model, we mention the question of whether the breakdown process has the character of a second or first order phase transition [17–20]. Central to this question is the question of the distribution of fuses that burn out simultaneously or—equivalently in the fiber bundle model—the number of fibers that fail simultaneously. This question was first raised and solved analytically in the context of the equal load-sharing fiber bundle [21] and then for the local load-sharing model [22]. The same question was first studied in connection with the fuse model in Ref. [23].

The particular problem we study here, elastic interfacial failure, has been addressed in the literature earlier by Delaplace and co-workers [13,24,25]. The system consists of two elastic media that have been welded together, thus sharing a common interface. In general, the media can have different elastic constants. However, for the sake of simplicity and without loss of generality, we assume one of the media to be infinitely stiff while the other is elastic. We can view this simplification as an effective representation of the original system since it does not change the physics. Furthermore, we assume that the “soft” medium is uniform with respect to its

*Permanent address: Department of Physics, NTNU, N-7491 Trondheim, Norway.

elastic properties; it has the same elastic properties everywhere. However, the local *strength* of the glue—defined as the maximum local load it may sustain without failing—varies from point to point along the interface. This is the source of disorder in the system. In real systems this disorder would typically be correlated. In this first attack on the problem, we assume the disorder to be uncorrelated. Our main interest here is to understand how correlations develop due to the failure process. In Sec. II we describe the numerical model in detail.

The two joined media are subjected to a progressive uniform load perpendicular to the glue interface. Local failures will develop in the interface that changes the stress field on the remaining intact interface. These changes in the stress field will compete with the local strength of the glue to determine where the next failure happens. Sometimes, a local failure will occur due to the glue being particularly weak at that point on the interface, other times failure will occur due to enhancements in the local stress field. This competition leads to the development of spatial correlations both in the stress field and in the failure patterns, and in the failure process itself.

The two media can be pulled apart by controlling (fixing) either the applied force or the *displacement*. The displacement is defined as the change in the distance between two points, one in each medium, positioned far from the glued interface. Clearly, the line connecting these points is perpendicular to the average position of the interface. In our case, the pulling is accomplished by controlling the displacement. As the displacement is increased very slowly, glued points will fail. Sometimes the failed regions are very small, other times the failed region is larger. Such events, when a large area fails “instantaneously” compared to the time scale at which the displacement is changed, are called bursts. One of the quantities of interest to us is the *burst distribution* [21] as the failure process evolves. We show in Sec. III A that this distribution follows a power law.

In Sec. III B, we investigate the scaling properties of the load and displacement of the system at the point when the failure process becomes unstable. This is the point at which any further increase of either load or displacement will lead to a catastrophic burst where all remaining glue fails. This point defines the *strength* of the interface, and the question we pose is how this scales with the system size.

We then investigate the geometrical properties of the failed regions at the point when catastrophic failure occurs in Sec. III C. We find that the area distribution of the failed regions follow a power law.

We present our conclusions and outlook for further work in Sec. IV.

II. MODEL

The system described in the Introduction is continuous: Two media, one elastic, the other infinitely stiff, are glued together thus forming a common interface. In order to treat this problem numerically, the continuum problem is replaced by a discrete one. In Sec. II A we describe the discrete

model, while the numerical algorithms are discussed in Sec. II B.

A. Description of model

We discretize the glued interface by replacing it with two two-dimensional square $L \times L$ lattices with periodic boundary conditions. The lower one represents the hard, stiff surface and the upper one the elastic surface. The nodes of the two lattices are matched (i.e., there is no relative lateral displacement). The glue is modeled by springs connecting opposing nodes in the two lattices. All these harmonic springs have the same spring constant (set to unity) but breaking thresholds randomly drawn from a uniform distribution between zero and one. The spacing between the springs is a in both the x and y directions. The force that each spring is carrying is transferred over an area of size a^2 to the soft surface. In other words, the spring is effectively attached to a square of area a^2 . As the two glued media are separated by controlling the displacement of the hard medium D the forces carried by the springs increases. When the force carried by a spring reaches its breaking threshold, it breaks irreversibly and the forces redistribute. The springs are, thus, broken one by one until the two media are no longer in mechanical contact. As this process is proceeding, the elastic body is of course deforming to accommodate the changes in the forces acting on it.

The equations governing the system are as follows. The force f_i carried by the i th spring is given by Hooke’s law,

$$f_i = -k(u_i - D), \quad (1)$$

where k is the spring constant and u_i is the deformation of the elastic medium at site i . All unbroken springs have $k = 1$ while a broken spring has $k = 0$. The quantity $(u_i - D)$ is, therefore, the length spring i was stretched. In addition, a force applied at a point on an elastic surface will deform this surface over a region whose extent depends on its elastic properties. This is described by the coupled system of equations,

$$u_i = \sum_j G_{i,j} f_j, \quad (2)$$

where the elastic Green function $G_{i,j}$ is given by [26,27]

$$G_{i,j} = \frac{1 - s^2}{\pi e a^2} \int_{-a/2}^{+a/2} \int_{-a/2}^{+a/2} \frac{dx' dy'}{|(x - x', y - y')|}. \quad (3)$$

In this equation, s is the Poisson ratio, e the elastic constant, and $|\vec{i} - \vec{j}|$ the distance between sites i and j . The indices i and j run over all L^2 sites. The integration over the area a^2 is done to average the force from the springs over this area. Strictly speaking, the Green function applies for a medium occupying the infinite half space. However, with a judicious choice of elastic constants, we may use it for a finite medium if its range is small compared to L , the size of the system.

By combining Eqs. (1) and (2), we obtain

$$(\mathbf{I} + \mathbf{KG})\vec{f} = \mathbf{K}\vec{D}, \quad (4)$$

where we are using matrix-vector notation. \mathbf{I} is the $L^2 \times L^2$ identity matrix, and \mathbf{G} is the Green function represented as an $L^2 \times L^2$ dense matrix. The constant vector \vec{D} is L^2 dimensional. The *diagonal* matrix \mathbf{K} is also $L^2 \times L^2$. Its matrix elements are either 1 for unbroken springs, or 0 for broken ones. Of course \mathbf{K} and \mathbf{G} do not commute (except initially when there are no broken springs).

Once Eq. (4) is solved for the force \vec{f} Eq. (2) easily yields the deformations of the elastic surface.

B. Numerical method: Fourier acceleration

Equation (4) is of the familiar form $\mathbf{A}\vec{x} = \vec{b}$. Since the Green function connects all nodes to all other nodes, the $L^2 \times L^2$ matrix \mathbf{A} is dense that puts severe limits on the size of the system that may be studied. There are direct, time consuming methods to deal with such matrices, see Ref. [28]. However, as we shall see, this problem may be circumvented and much more efficient methods may be employed such as the Conjugate Gradient algorithm (CG) [28,29].

The simulation proceeds as follows. We start with all springs present, each with its randomly drawn breakdown threshold. The two media are then pulled apart, the forces calculated using CG, and the spring that is the nearest to its threshold is broken, i.e., the matrix element corresponding to it in the matrix \mathbf{K} is zeroed. Then the new forces are calculated, a new spring broken, and so on until all springs have been broken and the media separated.

However, there are two problems that render the simulation of large systems extremely difficult. The first is that since \mathbf{G} is $L^2 \times L^2$ *dense* matrix, the number of operations per CG iteration scales like L^4 . Even more serious is the fact that as the system evolves and springs are broken, the matrix $(\mathbf{I} + k\mathbf{G})$ becomes very ill conditioned.

To overcome the problematic L^4 scaling of the algorithm we note that the Green function is diagonal in Fourier space. Consequently, doing matrix-vector multiplications using fast Fourier transform's (FFT's) the scaling is much improved and goes like $L^2 \ln(L)$. Symbolically, this can be expressed as follows:

$$(\mathbf{I} + \mathbf{KF}^{-1}\mathbf{FG})\mathbf{F}^{-1}\vec{f} = \mathbf{K}\vec{D}, \quad (5)$$

where \mathbf{F} is the FFT operator and \mathbf{F}^{-1} its inverse ($\mathbf{F}^{-1}\mathbf{F} = 1$). Since \mathbf{I} and \mathbf{K} are diagonal, operations involving them are performed in real space. With this formulation, the number of operations/iterations in the CG algorithm now scales like $L^2 \ln(L)$.

To overcome the runaway behavior due to the ill conditioning we need to precondition the matrix [29]. This means that instead of solving Eq. (5), we solve the equivalent problem

$$\mathbf{Q}(\mathbf{I} + \mathbf{KF}^{-1}\mathbf{FG})\mathbf{F}^{-1}\vec{f} = \mathbf{QK}\vec{D}, \quad (6)$$

where we simply multiplied both sides by the arbitrary, positive definite preconditioning matrix \mathbf{Q} . Clearly, the ideal

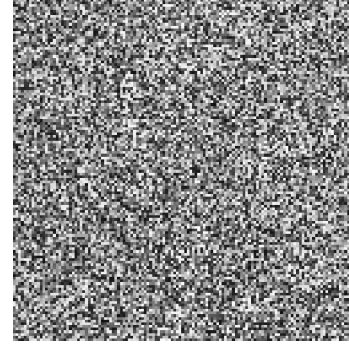


FIG. 1. Each elementary square represents a bond. The color scheme indicates when in the failure process a given bond failed, the lighter, the earlier. The lattice was 128×128 with an elastic constant $e = 10$.

choice is $\mathbf{Q}_0 = (\mathbf{I} + \mathbf{KG})^{-1}$, which would always solve the problem in one iteration. Since this is not possible in general, we look for a form for \mathbf{Q} that satisfies the following two conditions: (1) as close as possible to \mathbf{Q}_0 , and (2) fast to calculate. The choice of a good \mathbf{Q} is further complicated by the fact that as the system evolves and springs are broken, corresponding matrix elements of \mathbf{K} are set to zero. So, the matrix $(\mathbf{I} + \mathbf{KG})$ evolves from the initial form $(\mathbf{I} + \mathbf{G})$ to the final one \mathbf{I} . We were not able to find a fixed \mathbf{Q} that worked throughout the breaking process.

We therefore chose the form

$$\mathbf{Q} = \mathbf{I} - (\mathbf{KG}) + (\mathbf{KG})(\mathbf{KG}) - (\mathbf{KG})(\mathbf{KG})(\mathbf{KG}) + \dots, \quad (7)$$

which is nothing but the Taylor series expansion of $\mathbf{Q}_0 = (\mathbf{I} + \mathbf{KG})^{-1}$. For best performance, the number of terms kept in the expansion is left as a parameter, since it depends on the physical parameters of the system. It is important to emphasize the following points. (a) As springs are broken, the preconditioning matrix evolves with the ill-conditioned matrix and, therefore, remains a good approximation of its inverse throughout the breaking process. (b) All matrix multiplications involving \mathbf{G} are done using FFTs. (c) The calculation of \mathbf{Q} can be easily organized so that it scales like $nL^2 \ln(L)$ where n is the number of terms kept in the Taylor expansion, Eq. (7).

We therefore have a stable accelerated algorithm that scales essentially as the volume of the system. For example, for a 128×128 system, and taking $n = 5$, the CG algorithm always converges in four or five iterations with the prescribed precision of 10^{-12} .

III. RESULTS

We now present the results of our numerical simulations. We show in Fig. 1 a representation of the failure process. Each elementary square represents a spring (a bond), and the gray scale indicates when a particular spring failed: The darker the color, the earlier the failure. In this particular case, the elastic constant e was set to 10. There are no apparent spatial correlations between the failing bonds in this figure. However, we show in Fig. 2, the distance between succes-

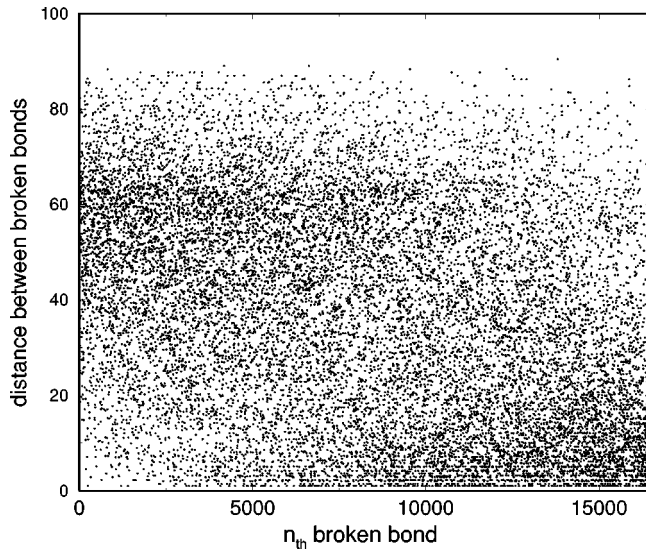


FIG. 2. Distance between successively broken bonds. The lattice was 128×128 with an elastic constant $e = 10$.

sively failing bonds for the same disorder realization of Fig. 1. We see clearly in this figure that early in the process there is no localization effect: Bonds tend to break far apart, the location being determined by the strength of bonds, i.e., early failure is disorder driven. However, halfway into the breakdown process, localization clearly develops. In Fig. 3, we show the corresponding plot for $e = 100$. In this case localization never develops for this size system and distribution of thresholds.

On the other hand, if the threshold distribution is much narrower than $[0,1]$ used above, localization can develop early. For example, we show in Fig. 4 the fracture graymap (like Fig. 1) for a uniform threshold distribution in the interval $[9.5,10.5]$. We clearly see the fracture starting towards the center of the figure and spreading out in a spiral till

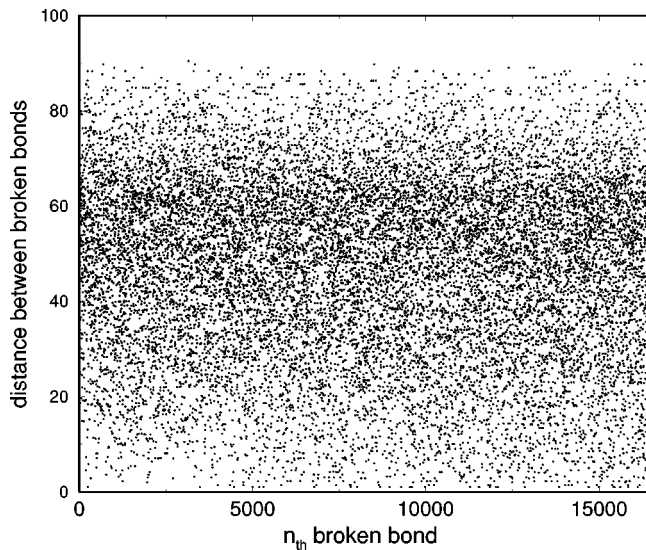


FIG. 3. Distance between successively broken bonds. The lattice was 128×128 with an elastic constant $e = 100$.

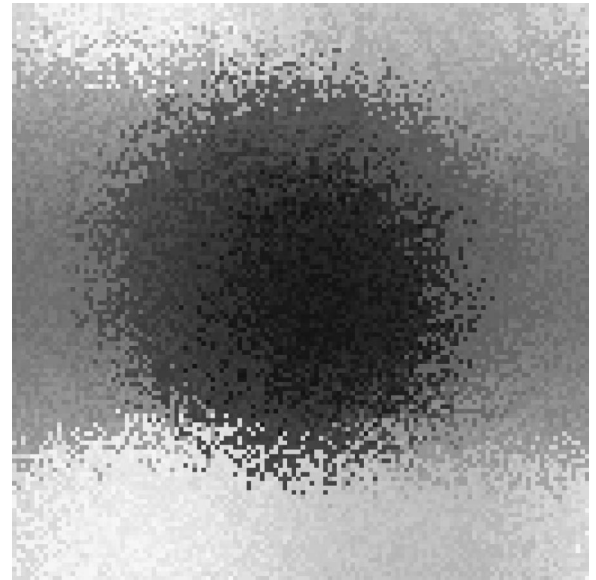


FIG. 4. Same as in Fig. 1 but with a narrow uniform threshold distribution in the interval $[9.5,10.5]$.

finally the symmetry is broken and the system ruptures along one of the lattice directions.

We note here that localization appears in Fig. 4 as a result of a narrow breaking threshold distribution. However, localization will also result as the ratio $ea/k \rightarrow 0$, where a is the distance between fibers. In other words, as the elastic medium softens, the system will approach the local load sharing model. This is a different mechanism from localization as a result of the narrowing of the threshold distribution.

Figure 5 shows the force-displacement curve for a system with elastic constant $e = 10$. Whether we control the applied force F or the displacement D the system will eventually suffer catastrophic collapse. However, this is not so when $e = 100$ as shown in Fig. 6. In this case, only controlling the force will lead to catastrophic failure. In the limit when $e \rightarrow \infty$, the model becomes the equal load-sharing fiber bundle model [1,2], where $F = (1 - D)D$. In this limit there are no

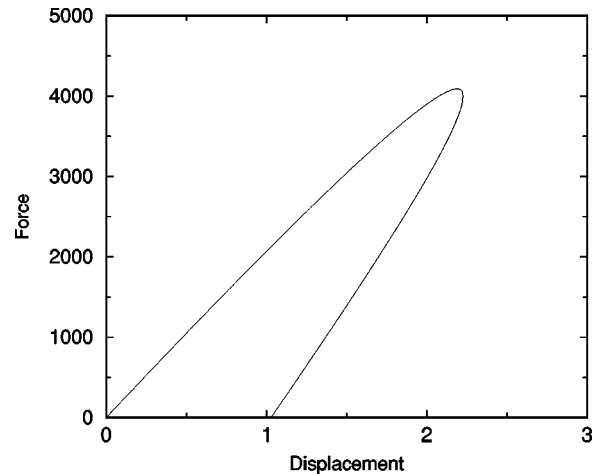


FIG. 5. Force-displacement curve, 128×128 systems with $e = 10$.

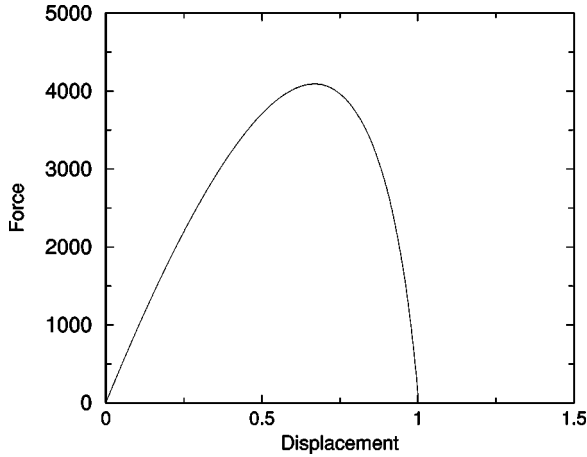


FIG. 6. Force-displacement curve, 128×128 systems with $e = 100$.

spatial correlations and the force instability is due to the decreasing total elastic constant of the system making the force on each surviving bond increase faster than the typical spread of threshold values. No such effect exists when controlling displacement D . However, when the elastic constant e is small, spatial correlations in the form of localization do develop, and these are responsible for the displacement instability that is seen in Fig. 5. In other words, the localization clearly visible in Fig. 2 starts to develop when the system is near the peak of its force-displacement curve, and dominates when the system is on the negative slope branch of that curve.

A. Burst distribution

We now turn to the study of the burst distribution. We define the size of a burst, Δ , in our model as the number of bonds that fail simultaneously while the force F is held constant. In the equal load-sharing fiber bundle model it has been shown that the burst distribution is given by [21]

$$N(\Delta, D) = \frac{1}{\Delta^\tau} n(\Delta^\sigma(x - x_c)) \quad (8)$$

where x_c is the damage, i.e., the density of broken bonds, at which the model fails catastrophically, n is a crossover function that approaches a constant when the argument approaches zero, and which falls off as $\exp(-y^2)$ as the argument y gets large. Furthermore,

$$\tau = \frac{5}{2} \quad \text{and} \quad \sigma = \frac{1}{2} \quad (9)$$

independent of the threshold distribution.

We show in Figs. 7 and 8 the burst distribution for $e = 10$ and 100 . In both cases we find that the burst distribution follows a power law with an exponent $\tau = -2.6 \pm 0.1$. We may argue that the exponent is the same as the one found in the equal loading fiber bundle, Eq. (9), $\tau = 5/2$ in the following way. The characteristics, $F = F(x)$ must have a quadratic

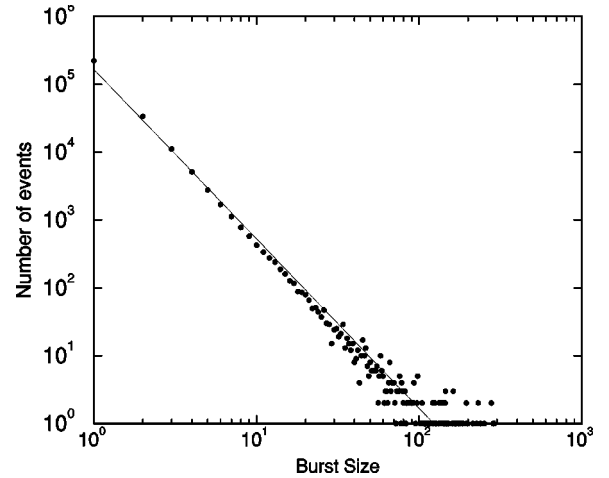


FIG. 7. Burst distribution for 128×128 , $e = 10$. The slope of the straight line is -2.5 .

maximum somewhere. For $e = 100$, such a maximum exists in the middle of failure process as seen in Fig. 8, whereas for $e = 10$, the system only approaches such a maximum near total failure, see Fig. 7. Assuming that the fluctuations about the average characteristics are Brownian—which can be shown analytically in the limit $e \rightarrow \infty$ [30–32]—near the maximum the probability to find a burst of size Δ is proportional to $\Delta^{-3/2} \exp[-\Delta(x - x_c)^2]$. This result comes from a mapping onto the *Gambler's ruin problem* [33]. Furthermore, in order to guarantee that the burst is not a burst within an even larger burst, the starting point of the burst must be the highest point on the characteristics that has occurred so far in the failure process. This condition may also be mapped onto the Gambler's ruin problem, and leads to an extra factor $(x - x_c)$ in the probability for a burst to occur. The probability to find a burst of size Δ throughout the failure process is then the integral over x as x approaches x_c , $\int^x dx (x - x_c) \Delta^{-3/2} \exp[-\Delta(x - x_c)^2]$ that is proportional to $\Delta^{-5/2}$. As can be seen in Figs. 7 and 8, the numerical data are consistent with the expected value $\tau = 5/2$.

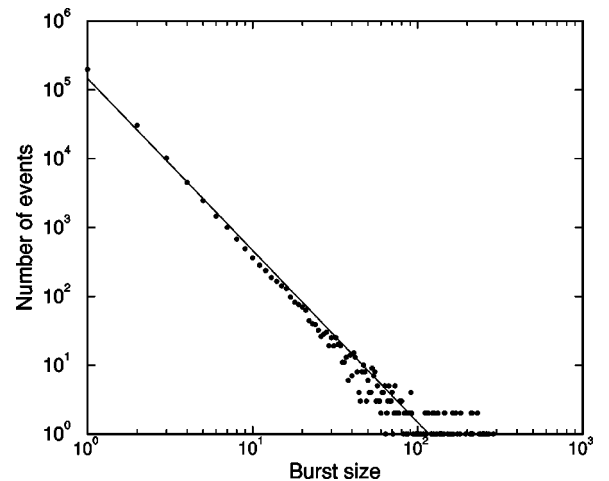


FIG. 8. Burst distribution for 128×128 , $e = 100$. The slope of the straight line is -2.5 .

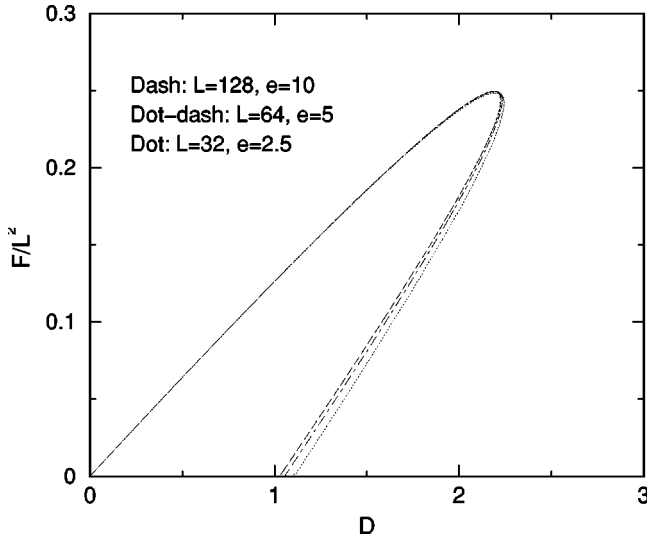


FIG. 9. Scaling of the failure characteristics for systems with $L = 128 (e = 10)$, $64 (e = 5)$, and $32 (e = 2.5)$ using the reduced variables $F/L^{2.0}$ and $D/L^{0.0}$.

B. Strength scaling

The load-displacement curves for different system sizes L coincide when we use the reduced variables F/L^a and D/L^b where $a = 2.0$ and $b = 0.0$, as seen in Fig. 9. We expect the exponent $a = 2$ since F/L^2 is the normal stress on the surface. In the case of an infinitely stiff system, we expect $b = 0$. The elastic system studied here behaves in the same way as long as the elastic constant e is also scaled with L . For example, for $L = 128$ we took $e = 10$, for $L = 64$ e should take half that value in order to reproduce the physics. This is easy to understand considering the dependence of the Green function, Eq. (3), on the elastic constant.

C. Spatial damage distribution at failure

As the failure process proceeds, there is an increasing competition between local failure due to stress enhancement and local failure due to local weakness of material. As we saw above, when we control the displacement D and e is sufficiently small (for example, $e = 10$), catastrophic failure eventually occurs due to localization. The onset of this localization, i.e., the catastrophic regime, occurs when the two mechanisms are equally important. One may suspect that criticality due to self organization [34] occurs at this point. In order to test whether this is the case, we have measured the size distribution of broken bond clusters at the point when D reaches its maximum point on the $F-D$ characteristics, i.e., the onset of localization and catastrophic failure. The analysis was performed using a Hoshen-Kopelman algorithm [35]. We show the result in Fig. 10, for 56 disorder realizations, $L = 128$ and $e = 10$. The result is consistent with a power law distribution with exponent -1.6 , and consequently with self-organization.

IV. CONCLUSION

We have studied numerically the failure of the glued interface between an elastic and an infinitely stiff blocks of

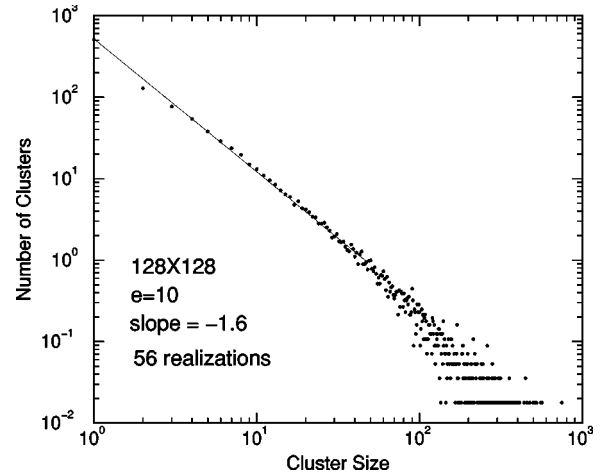


FIG. 10. Area distribution of zones where glue has failed for systems of size 128×128 and elastic constant $e = 10$. The straight line is a least square fit and indicates a power law with exponent -1.6 . $e = 10$

material. To this end we have developed a stable and accelerated algorithm that scales $L^2 \ln(L)$ that enabled us to study much bigger systems than previously possible.

Our main physical results are: For a uniform threshold distribution on the unit interval we find (1) the distribution of simultaneously failing glue (bursts) is a power law with exponent -2.6 ± 0.1 that is consistent with the burst distribution found in the equal load-sharing fiber bundle problem. (2) The point of catastrophic failure scales as L^2 in force and L^0 in displacement. (3) The area distribution of failed regions (clusters) at the onset of catastrophic failure when displacement is the control parameter is consistent with a power law with an exponent equal to -1.6 . This hints at self-organization.

We should note here that the conclusion in point (2) above may be altered as a result of changing, e.g., the threshold distribution or e , see [36] for a study of these questions on a related model.

In addition to the above observations, we saw that for large e , e.g., $e = 100$, the system does not suffer catastrophic failure, and there is no localization. On the other hand, smaller values of e , e.g., $e = 10$, resulted in catastrophic failure due to localization. By doing the simulations for various values of e we estimate that failure due to localization starts to occur for $e \sim 35-40$. As we will see below, these values of e obtained for 128×128 systems should be scaled appropriately when the size of the system is changed.

The disorder in our system was uncorrelated. As mentioned above, it is realistic to introduce correlations as exist, for example, in fracture surfaces. This can be done by generating spring breaking thresholds that have the desired correlations. Furthermore, we have used a flat distribution for the disorder. One can use other distributions, e.g., r^α , where r is a uniformly distributed random number and α an exponent that can be negative. It is known from random fuse models of fracture that the breakdown process depends on the value of α . It is not clear how these issues will modify our current results. This work is in progress.

Another work in progress is to study the propagating fracture front when the above glued media are ripped apart by pulling only on one side of the $L \times L$ square system. As before the breaking thresholds can be correlated or uncorrelated. These results will also be compared with the results of experiment currently underway.

Finally, we have chosen to introduce disorder into the breaking thresholds of the springs. However, we can just as easily introduce it into the spring constants themselves, again with or without correlations.

ACKNOWLEDGMENTS

We thank F. A. Oliveira and H. Nazareno and the ICCMP of the Universidade de Brasília for warm hospitality and support during the initial phases of this work. This work was partially funded by the CNRS PICS through Contract No. 753 and the Norwegian Research Council, NFR. We also thank NORDITA for its hospitality and further support. A.H. thanks the Niels Bohr Institute for support and hospitality during his sabbatical year.

-
- [1] F.T. Peirce, *J. Text. Inst.* **17**, 355 (1926).
 - [2] H.E. Daniels, *Proc. R. Soc. London, Ser. A* **183**, 405 (1945).
 - [3] D.G. Harlow and S.I. Phoenix, *J. Compos. Mater.* **12**, 195 (1978).
 - [4] D.G. Harlow and S.I. Phoenix, *J. Compos. Mater.* **12**, 314 (1978).
 - [5] D.G. Harlow and S.I. Phoenix, *Int. J. Fract.* **17**, 601 (1981).
 - [6] D. Harlow, *Proc. R. Soc. London, Ser. A* **397**, 211 (1985).
 - [7] D.G. Harlow and S.L. Phoenix, *J. Mech. Phys. Solids* **39**, 173 (1991).
 - [8] P.M. Duxbury and P.L. Leath, *Phys. Rev. B* **49**, 12 676 (1994).
 - [9] W.I. Newman and S.L. Phoenix, *Phys. Rev. E* **63**, 021507 (2001).
 - [10] W.I. Newman and A.M. Gabrielov, *Int. J. Fract.* **50**, 1 (1991).
 - [11] S.-d. Zhang, Z.-q. Huang, and E.-j. Ding, *Phys. Rev. E* **54**, 3314 (1996).
 - [12] A. Delaplace, G. Pijaudier-Cabot, and S. Roux, *J. Phys. IV* **8**, 103 (1998).
 - [13] A. Delaplace, Doctoral thesis, Ecole Normale Supérieure, Cachan, 1999.
 - [14] H. J. Herrmann and S. Roux, *Statistical Models for the Fracture of Disordered Media* (North-Holland, Amsterdam, 1990).
 - [15] A. Hansen, in *Physical Aspects of Fracture*, edited by E. Bouchaud (Kluwer Academic Publishers, Dordrecht, 2001).
 - [16] R.L. Smith and S.L. Phoenix, *ASME J. Appl. Mech.* **48**, 75 (1981).
 - [17] S. Zapperi, A. Vespignani, and H.E. Stanley, *Nature (London)* **388**, 658 (1997).
 - [18] S. Zapperi, P. Ray, H.E. Stanley, and A. Vespignani, *Phys. Rev. E* **59**, 5049 (1999).
 - [19] Y. Moreno, J.B. Gómez, and A.F. Pacheco, *Phys. Rev. Lett.* **85**, 2865 (2000).
 - [20] A. Johansen and Sornette, *Eur. Phys. J. B* **18**, 163 (2000).
 - [21] P.C. Hemmer and A. Hansen, *ASME J. Appl. Mech.* **59**, 909 (1992).
 - [22] M. Kloster, A. Hansen, and P.C. Hemmer, *Phys. Rev. E* **56**, 2615 (1997).
 - [23] A. Hansen and P.C. Hemmer, *Phys. Lett. A* **184**, 394 (1994).
 - [24] A. Delaplace, S. Roux, and G. Pijaudier-Cabot, *Int. J. Solids Struct.* **36**, 1403 (1999).
 - [25] S. Roux, A. Delaplace, and G. Pijaudier-Cabot, *Physica A* **270**, 35 (1999).
 - [26] L. Landau and E. M. Litshitz, *Theory of Elasticity* (Clarendon Press, Oxford, 1958).
 - [27] K. L. Johnson, *Contact Mechanics* (Cambridge University Press, Cambridge, 1985).
 - [28] W. H. Press, S. A. Teukolsky, W. T. Vetterling, and B. P. Flannery, *Numerical Recipes in Fortran 77: The Art of Scientific Computing* (Cambridge University Press, Cambridge, 1992).
 - [29] G.G. Batrouni and A. Hansen, *J. Stat. Phys.* **52**, 747 (1988).
 - [30] S.L. Phoenix and H.M. Taylor, *Adv. Appl. Probab.* **5**, 200 (1973).
 - [31] H.E. Daniels and H.T.R. Skyrme, *Adv. Appl. Probab.* **17**, 85 (1985).
 - [32] H.E. Daniels, *Adv. Appl. Probab.* **21**, 315 (1989).
 - [33] A. Hansen and P.C. Hemmer, *Trends Stat. Phys.* **1**, 213 (1994).
 - [34] P. Bak, C. Tang, and K. Wiesenfeld, *Phys. Rev. Lett.* **59**, 381 (1987).
 - [35] D. Stauffer and A. Aharony, *Introduction to Percolation Theory* (Taylor and Francis, London, 1994).
 - [36] S. Mahesh, I.J. Beyerlein, and S.L. Phoenix, *Physica D* **133**, 371 (1999).